Received: 1 September 2020 | Revised: 17 January 2021 | Accepted: 18 January 2021

DOI: 10.1002/gj.4096

SPECIAL ISSUE ARTICLE

WILEY

Biostratigraphic significance and geometric morphometrics of *Euestheria gutta* (Crustacea: Branchiopoda: Spinicaudata): An index fossil of continental Permian–Triassic transitional beds

Xue Miao[1] | Daoliang Chu[1] | Jinnan Tong[1] | Michael J. Benton[2] | Jianxin Yu[1] | Liang Luo[3] | Wenchao Shu[1] | Yuyang Wu[1]

[1]State Key Laboratory of Biogeology and Environmental Geology, School of Earth Sciences, China University of Geosciences, Wuhan, China

[2]School of Earth Sciences, University of Bristol, Bristol, UK

[3]Chengdu Center of China Geological Survey, CGS, Chengdu, China

Correspondence
Daoliang Chu, State Key Laboratory of Biogeology and Environmental Geology, School of Earth Sciences, China University of Geosciences, Wuhan 430074, China.
Email: chudl@cug.edu.cn

Funding information
China Geological Survey, Grant/Award Numbers: CDD2001-03, DD20190009; National Natural Science Foundation of China, Grant/Award Numbers: 41702015, 41802031, 42072025

Handling Editor: Z.-Q. Chen

The Permian–Triassic mass extinction was the largest biotic extinction event in the Phanerozoic and affected both marine and continental life. Marine Permian–Triassic transitional sequences can be correlated in many regions, but this has proved difficult for continental successions. A growing number of studies show that spinicaudatans are some of the most common fossils in continental strata and can be used as index fossils for continental stratigraphic division and correlation. Here we document the morphology and biostratigraphic significance of *Euestheria gutta* based on well-preserved fossils from southwestern China. It shows strong intraspecific morphological variation, while the most important feature is the strongly convex larval valve and significant finely pitted to weakly reticulated ornamentation on the growth bands. Evidence from palaeobotany, charcoal, and organic carbon isotopes indicated that the continental mass extinction in southwestern China was marked by the catastrophic loss of tropical rainforest vegetation, enhanced wildfire and a negative carbon isotope excursion (CIE) during the P–Tr transition. Meanwhile, abundant *E. gutta* first appeared at the onset of the negative CIE and just above the horizon of the loss of macroflora. Based on the global geographic distribution of *E. gutta* and temporal correlation, we conclude that this species existed from the latest Permian to the earliest Triassic, and the occurrence of *E. gutta* could be used as an index fossil of the continental mass extinction interval or P–Tr transitional beds.

KEYWORDS
Euestheria gutta, palaeogeographical distribution, palaeoecology, Permian–Triassic transition, Spinicaudatan

1 | INTRODUCTION

Numerous studies have focused on biotic and environmental changes during the Permian–Triassic (P–Tr) transition, and they suggest that this greatest mass extinction event severely affected both marine and continental ecosystems (e.g., Benton, 2015; Erwin, 2006). However, there has been no consensus on whether the mass extinctions of marine and continental life during the P–Tr biotic crisis were synchronous or not (e.g., Cao, Wang, Liu, Shen, & Summons, 2008; Chu et al., 2020; Fielding et al., 2019; Nowak, Schneebeli-Hermann, & Kustatscher, 2019; Twitchett, Looy, Morante, Visscher, & Wignall, 2001). Several killing agents for this crisis have been proposed (e.g. Joachimski et al., 2012; Wignall & Hallam, 1992), especially extreme environmental stress linked to the effects of the Siberian Traps eruptions on the basis of the rough temporal coincidence of the two events (Burgess, Muirhead, & Bowring, 2017; Grasby, Sanei, & Beauchamp, 2011; Wignall, 2001). Hitherto, P–Tr transitional marine biostratigraphy, chemostratigraphy, and chronostratigraphy have been

widely investigated on a global scale (e.g., Burgess, Bowring, & Shen, 2014; Chen et al., 2015; Chen & Xu, 2019; Song, Wignall, Tong, & Yin, 2013). However, it is very difficult to test the age of continental successions because of the absence of age-diagnostic fossils or other indices (Tong et al., 2019). Multidisciplinary studies have focused on correlations of continental P–Tr stratigraphic sections such as a vertebrate fossil-based biostratigraphic scheme (Benton, Tverdokhlebov, & Surkov, 2004; Lucas, 2006, 2010; Schneider et al., 2020; Smith & Ward, 2001; Viglietti et al., 2016), geomagnetic polarity (Gastaldo et al., 2015; Gastaldo, Knight, Neveling, & Tabor, 2014; Steiner, 2006; Szurlies, 2007, 2013; Taylor et al., 2009), carbon isotopes (Cao et al., 2008; Metcalfe, Crowley, Nicoll, & Schmitz, 2015; Shen et al., 2011; Ward et al., 2005; Wu et al., 2020; Zhang et al., 2016), and high-precision dating (Fielding et al., 2019; Gastaldo et al., 2020; Metcalfe et al., 2015; Shen, Sun, Lin, Liu, & Chai, 2011). However, the definition and position of the P–Tr boundary (PTB) in non-marine basins is disputed, such as the conflicting opinions on the vertebrate-defined PTB in the Karoo Basin of South Africa (Botha & Smith, 2006; Gastaldo et al., 2015, 2020; Neveling et al., 2016; Smith & Ward, 2001; Ward et al., 2005).

The correlation between marine and continental P–Tr transitional strata is crucial for a comprehensive understanding of global biotic and environmental responses (Tong et al., 2019), though this is difficult because the fossil assemblages are different. Recently, marine-continental transitional siliciclastic settings were considered to be a possible means to correlate marine and continental sections (Chu et al., 2016; Chu, Tong, Benton, Yu, & Huang, 2019; Peng et al., 2005; Peng & Shi, 2009; Shen, Crowley, et al., 2011; Wignall et al., 2020; Zhang et al., 2016). In addition, the biotic and environmental events around the PTB were also considered as useful tools for correlation between marine and continental deposits (Tong et al., 2019). A negative carbon isotope excursion (CIE) associated with the major floral and faunal turnovers was observed globally in both carbonate and organic matter at the PTB, and this provides a correlation tool between the continental and marine records (e.g., Korte & Kozur, 2010 and Wu et al., 2020; references therein).

Spinicaudatans are a group of small branchiopod crustaceans. Extant spinicaudatans are key components of ephemeral freshwater pools, and they occur worldwide in ephemeral parts of astatic lakes in endorheic basins (Jones, 1862; Martínez-Pantoja, Alcocer, & Maeda-Martínez, 2002). However, fossil spinicaudatans could also live in permanent water bodies, such as stable lakes, in the Palaeozoic and Mesozoic (Hethke et al., 2019; Scholze, Schneider, & Werneburg, 2016). Their chitinous carapace was strong and stable to resist damage during life, and this means that the fossils can survive in good condition through destructive taphonomic processes (Astrop, Sahni, Blackledge, & Stark, 2015). Spinicaudatans are some of the most common fossils in continental strata since the Devonian, and their wide distribution and fast evolution means they can be used as effective tools for continental stratigraphic division and correlation (Huang, 2019; Kozur & Weems, 2010; Morton, Whiteside, Hethke, & Benton, 2017; Schneider et al., 2020; Schneider & Scholze, 2016; Tasch & Volkheimer, 1970). Recently, spinicaudatan biostratigraphy has been attempted for continental P–Tr transitional strata, based on their worldwide distribution, including Russia, western Europe, northwestern China, and South China (Chu et al., 2016; Chu, Tong, Yu, Song, & Tian, 2013; Kozur & Weems, 2011; Schneider et al., 2020; Schneider & Scholze, 2016; Scholze et al., 2015; Scholze et al., 2016; Scholze, Golubev, Niedźwiedzki, Schneider, & Sennikov, 2019). In particular, some species were discovered in the latest Permian, earliest Triassic, or Permian–Triassic transitional strata from various basins, such as South China, North China, Germanic Basin, and Moscow Syncline (Chu et al., 2016; Chu et al., 2019; Kozur & Seidel, 1983a, 1983b; Scholze et al., 2015; Scholze et al., 2016). And they may be of biostratigraphic significance. In particular, *Euestheria gutta* has been reported repeatedly and shows potential as the index fossil of P–Tr transitional strata, though the time range of this species has been debated, as it has been thought to be latest Permian, earliest Triassic, or Permian–Triassic transitional in age (Chu et al., 2013; Chu et al., 2016; Scholze et al., 2015; Scholze et al., 2016; Scholze et al., 2019). Herein, we explore the biostratigraphic significance of *E. gutta* and the temporal relationship between occurrences of this species and other fossils based on well-preserved records from southwestern China. We examine bulk-sediment organic carbon isotopes to establish chemostratigraphy and indicate the horizon of the biotic and environmental crisis through the P–Tr transition in the studied sections. Additionally, this article will clarify the detailed morphological features of *E. gutta*.

2 | GENERAL LITHOSTRATIGRAPHY

We collected fossils from the Chahe, Jinzhong, and Chinahe sections in an adjoining area between western Guizhou and eastern Yunnan in southwestern China (Figure 1). During the Late Permian and Early Triassic, South China was located within the Palaeo-Tethys Ocean at equatorial palaeolatitudes (Muttoni et al., 2009). There is a gradual change from continental to shallow marine facies recorded in an almost continuous outcrop from southwestern China (Figure 1; e.g., Chu et al., 2016; Peng et al., 2005; Shen, Crowley, et al., 2011). The continental latest Permian to earliest Triassic strata in southwestern China comprise the Xuanwei, Kayitou, and Dongchuan formations, in ascending order. The Xuanwei Formation (Late Permian) is represented by greenish fine- to coarse-grained sandstone and dark grey laminated or massive mudstone with coal beds or seams which contains a large number of members of the *Gigantopteris* flora. The Kayitou Formation (latest Permian to earliest Triassic) is similar to the underlying Xuanwei Formation but lacks coal due to the loss of tropical rain forests, and it contains a large number of animal fossils, such as spinicaudatans, and even bivalves and brachiopods in continental-marine transitional facies of the Jinzhong Section, which can correlate with the Feixianguan Formation (Chu et al., 2016). The Dongchuan Formation (Early Triassic) is composed of massive purple-red cross-bedded sandstones, siltstones with thinly interbedded mudstones, which contains very few fossils and over 800 m in thickness

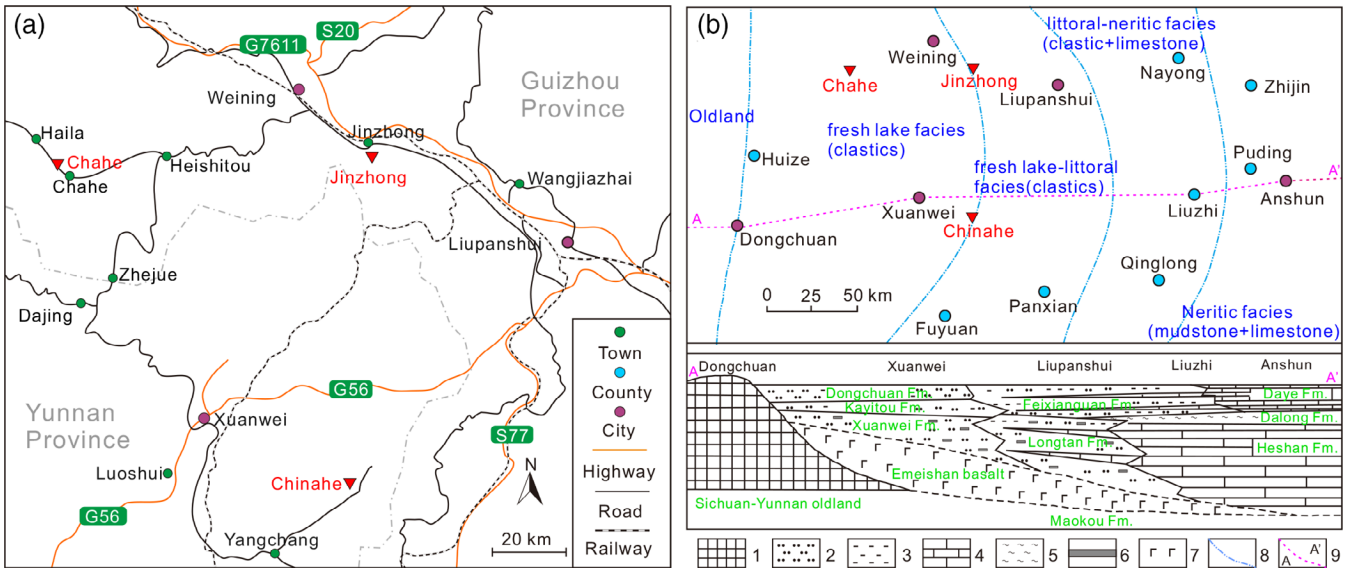

FIGURE 1 Location map of the studied sections (a) and the palaeogeography and lithostratigraphy of western Guizhou and eastern Yunnan during the P–Tr transition (b, modified after Peng et al., 2005). 1, oldland; 2, sandstone and/or siltstone; 3, mudstone; 4, limestone; 5, chert; 6, coal; 7, basalt; 8, facies boundary; 9, A to A' cross-section line

(Figure 7). Previous studies suggested that the Kayitou Formation records the mass extinction of the *Gigantopteris* flora and the turnover of the sedimentary system associated with the climate change, which corresponds to the P–Tr transitional interval (e.g., Bercovici, Cui, Forel, Yu, & Vajda, 2015; Chu et al., 2016; Zhang et al., 2016).

2.1 | Chahe section

This roadcut section is located in Chahe Town, Weining County, western Guizhou Province (Figure 1). It exposes sandstone, mudstone, and coal beds of the Xuanwei Formation, the overlying Kayitou Formation which is dominated by brownish-yellow mudstone without coal, and the Dongchuan Formation which is composed of purple-red sandstone. Previous studies proposed that there was a sharp and severe floral extinction event in the lower part of the Kayitou Formation (e.g., Chu et al., 2016; Zhang et al., 2016).

2.2 | Jinzhong section

The Jinzhong section, located in Jinzhong Town, Weining County, western Guizhou Province (Figure 1), exposes the upper part of the Xuanwei Formation, the Kayitou Formation, and the lower part of the Dongchuan Formation in ascending order. The Xuanwei Formation is dominated by sandstone, mudstone and coal beds. The *Gigantopteris* flora was commonly observed below the uppermost coal. The Kayitou Formation corresponds to a shallow coastal lagoon evolving towards coastal transitional deposition, yielding a continental-marine mixed biota including plants, spinicaudatans, bivalves, and brachiopods (Chu et al., 2016).

2.3 | Chinahe section

The Chinahe section is located in Tianba town, Xuanwei city, eastern Yunnan Province. It exposes the entire Xuanwei Formation overlying the Emeishan Basalt, the Kayitou Formation, and the Feixianguan Formation. The Xuanwei Formation is dominated by sandstone, mudstone, and coal, with abundant *Gigantopteris* flora plants. The grey–green mudstone of the Kayitou Formation possesses a similar mixed continental-marine biota as the Jinzhong section (Song, Tong, Tian, Chu, & Huang, 2019).

3 | MATERIALS AND METHODS

Abundant well-preserved *E. gutta* were collected in the Kayitou Formation of the studied sections (Figure 2). These were examined and photographed using the method of Chu et al. (2016). A serious problem in a study of this kind is that a large number of synonymous or invalid species of spinicaudatans have been reported because of problems with descriptive terminologies, limited morphological features of the carapace, intraspecific variation and poorly preserved specimens (see discussion in Scholze et al., 2015). Without an agreed taxonomy, a spinicaudatan biostratigraphy is hard to establish. Therefore, we use quantitative and semi-quantitative carapace measurements (Hethke, Fürsich, Morton, & Jiang, 2018; Scholze et al., 2015) to describe *E. gutta*. Nine linear measurements from each specimen were made using digitization tools in the illustration package CorelDRAW X4 (Figure 3a), including carapace length (L), carapace height (H), length of the dorsal margin (Ch), the horizontal distance between the posterior dorsal extremity and the posterior-most point of the carapace (Arr), the horizontal distance between the anterior dorsal extremity

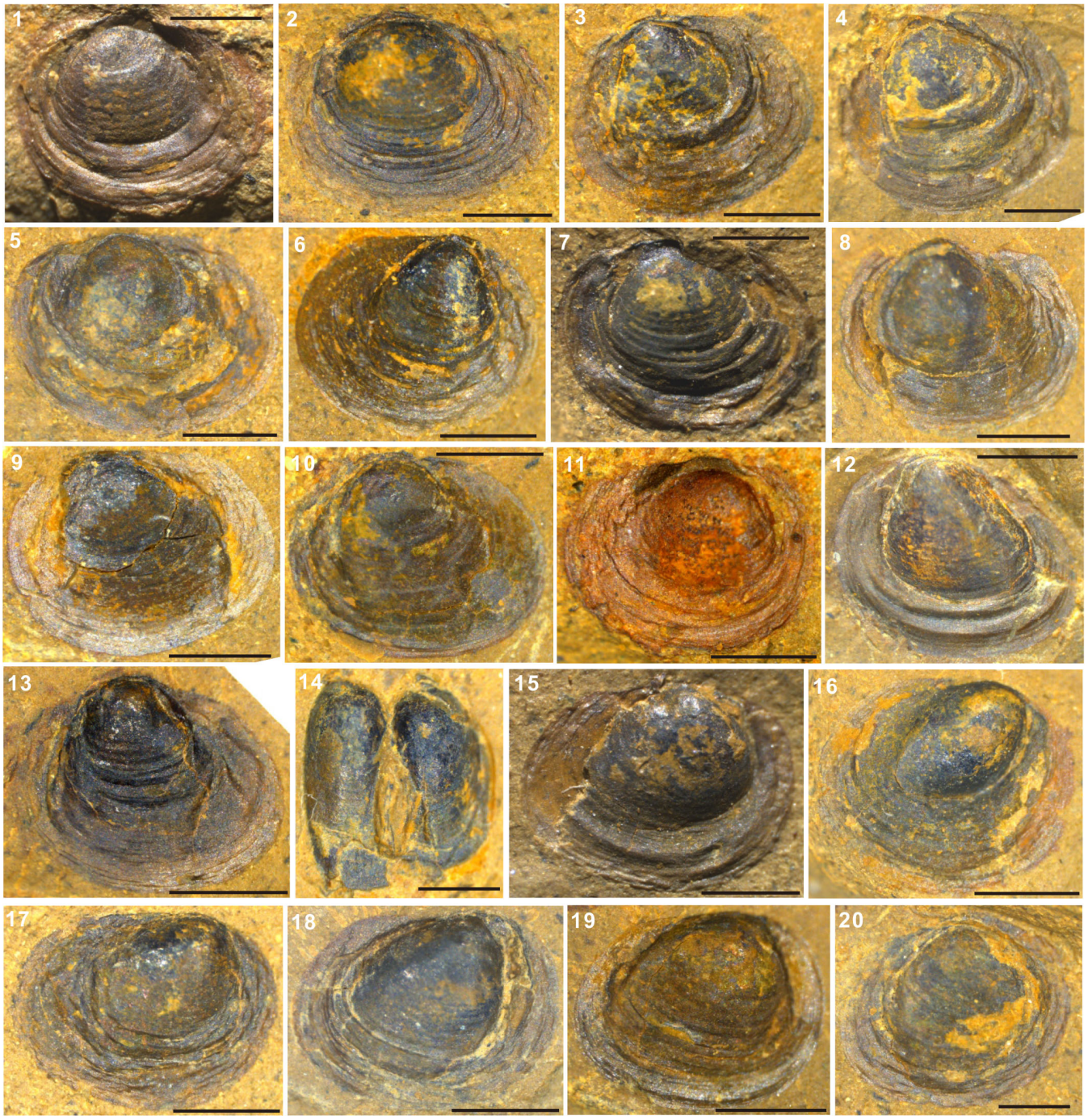

FIGURE 2 *E. gutta* from the Kayitou Formation of the studied sections. 1–13 (except 6, 11), cast of left valves; 14, cast of left and right valves of the same specimen; 6, 11, 15–20, cast of right valves. 1–8, 13–15 from Chinahe section; 9–12, from Chahe section; 16–20 from Jinzhong section. All scale bars represent 1 mm

and the anterior-most point of the carapace (Av), the horizontal distance between the highest point of the umbo and the anterior-most point of the carapace (Cr), the vertical distance between the anterior dorsal extremity and the anterior-most point of the carapace (a), the vertical distance between the posterior dorsal extremity and the posterior-most point of the carapace (b), and the horizontal distance between the lowest point on the ventral margin and the anterior-most point on the carapace (c) (Defretin-Lefranc, 1965; Tasch, 1987). Fourier shape analysis was an appropriate approach to analyse the shape of spinicaudatans by measuring the outline. The 76 specimens of *E. gutta* from Southwestern China (present study), the Germanic Basin (Kozur & Seidel, 1983a; Scholze et al., 2015), and the Moscow Syncline (Scholze et al., 2015; Scholze et al., 2016) were selected for morphometric studies. It is difficult to define genetically homologous points on a spinicaudatan carapace to use fixed landmarks (Haines & Crampton, 2000), so we used outline analysis instead. Left valves

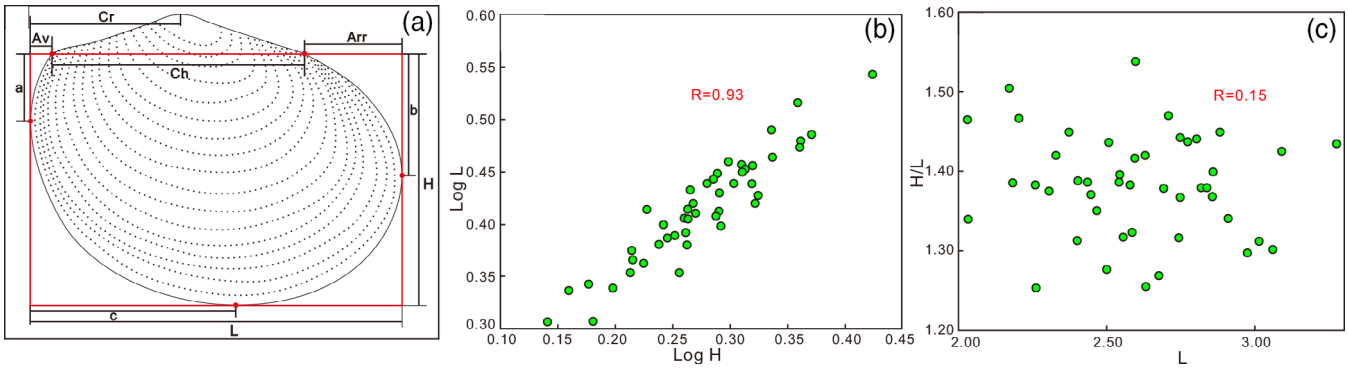

FIGURE 3 Linear measurements (see text for explanation). (a) Positions of nine linear measurements on a spinicaudatan carapace (modified after Hethke et al., 2018); (b) carapace length versus carapace height, data are log-transformed; (c) carapace length/height (a proxy for elongation of circularity) versus length

were mirrored for the analysis. The posterior dorsal extremity was used as the starting position, considering that it is easy to identify the position and can minimize the effect of an unclear position of the outline in automatic tracing. The entire carapace outline was transformed into 2,000 x and y co-ordinates using the digitization software tpsDig2 for Fourier shape analysis (Rohlf, 2010). A series of Fourier coefficients of these co-ordinates were obtained, and the statistics were transformed by the HANGLE Fourier function with 10 smoothing iterations in PAST (Haines & Crampton, 2000). The first 10 harmonics of the Fourier coefficients were used, which convert the original co-ordinate data into a series of harmonics (see Supplementary material). Then the data were processed and analysed for principal components analysis (PCA) on a variance–covariance matrix using the program PAST. Finally, a one-way non-parametric MANOVA (NPMANOVA) test was used to check the distinctions of the three groups.

In preparation for bulk organic carbon isotope analyses, each sample was powdered (< 200 mesh). Up to 2 g of sample was placed in a centrifuge tube, and then reacted with 3 mol/L HCl for 24 h to remove carbonate mineral phases. Then samples were rinsed with ultrapure water repeatedly until neutralized, and finally dried at 35°C. The treated samples were measured on an elemental analyser (EA) coupled with an isotope ratio mass spectrometer (Thermo Delta V Advantage) at the State Key Laboratory of Biogeology and Environmental Geology of the China University of Geosciences (Wuhan). All organic carbon isotope values are reported as in per mill relative to VPDB. The results were calibrated using USGS standards and the analytical precision was reproducible to better than ±0.2‰.

4 | RESULTS

4.1 | Morphological features of *Euestheria gutta*

4.1.1 | Linear measurements and ornamentation

The linear measurements show significant intraspecific variation, which is larger in the values of Cr, Av, and Arr, and smaller in L and H (see Supplementary material for the detailed linear measurements data). These suggest variable measures in the position of the umbo and dorsal margin length. A highly significant positive correlation between height and length is observed (r = 0.93, $p < 0.02$, Figure 3b), but there is no evidence for a correlation between length/height (a proxy for elongation of circularity) and length (r = 0.15, $p > 0.45$, Figure 3c).

Well-preserved specimens show carapace ornamentation on the growth bands (Figure 4). The finely pitted to weakly reticulated ornament is surrounded by pits and a raised mesh which shows weakly interconnected polygons on each growth band (Figure 4).

4.1.2 | Fourier shape analysis

In the PCA of the 76 specimens of *E. gutta* in three regions (Figure 5), variables PC1 to PC6 represent the vast majority of shape change, and they explain 26.5, 17.2, 14.2, 9.5, 9.0, and 7.9% of the total variation in the dataset comprising 18 Fourier coefficients for each outline. Here we focus on PC1–3, which account for 57.9% of variation. There are varying degrees of overlap among the three clusters by PCA. Specimens FS-2015-9C and FS-2015-9D fall outside of the main interval of the green cluster on both plots (Figure 5a,b), and their dorsal margins are relatively straight, the positions of the umbo supramarginal, which suggests that PC1 scores indicate the shape of the dorsal margin and the position of the umbo. In addition, PC1 reveals that the Southwestern China specimens differ considerably from those from the Germanic Basin and Moscow Syncline, which may indicate significant regional features, that is, the position of the umbo is more prominent above the dorsal margin. PC2 represents the posterior or anterior margin, and the distribution of specimens shows only a modest spread (Figure 5a). In the plot of PC1 versus PC3 (Figure 5b), there was no clear distinction of the three clusters along PC3, which indicates the shape of the ventral margin. Further, the *p*-values show significant differences between these three groups (values <0.01; Supplementary material).

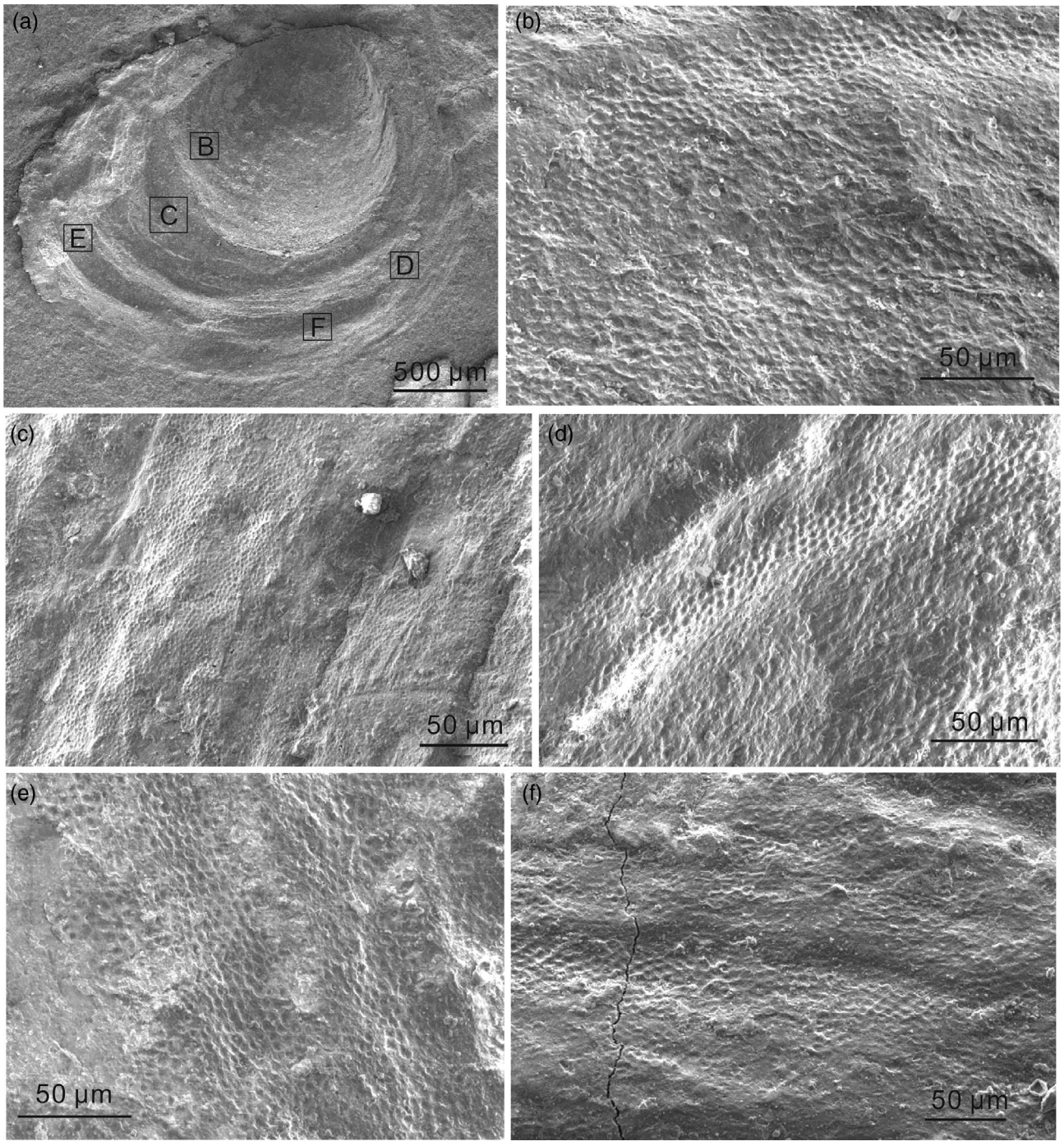

FIGURE 4 SEM images showing finely pitted to weakly reticulated microsculptures on growth bands

Summarizing, there is strong intraspecific morphological variation among the *E. gutta* specimens from the different regions, and the difference in the shape of the dorsal margin is most significant. This kind of morphological variability has also been reported in modern Spinicaudata (Hethke & Weeks, 2020). Compared to the specimens from the Germanic Basin and Moscow Syncline, the *E. gutta* specimens from Southwestern China show a more prominent dorsal margin, which represents a regional characteristic.

4.1.3 | Descriptive terminology

Description

The carapace is small- to medium-sized (length 2–3 mm, height 1.5–2 mm) and oval-round in shape (H/L = 0.7–0.8); dorsal marginal short (Ch/L = 0.45–0.65) and straight to slightly curved; larval valve small to large, and very strongly convex; position of the umbo is submedial and marginal or anterior and inframarginal;

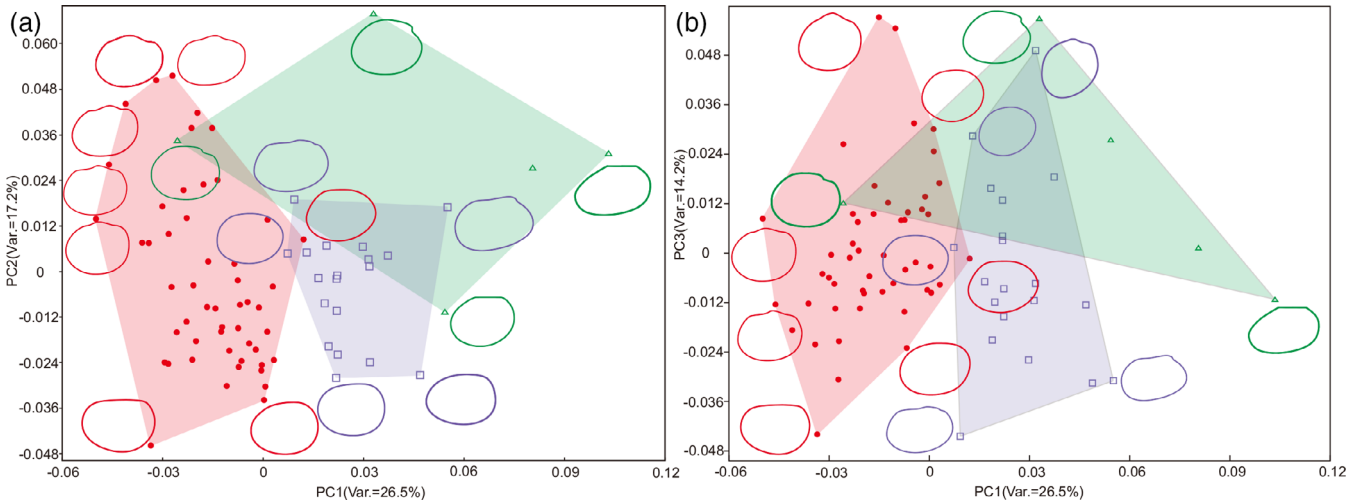

FIGURE 5 Plots of PC1, PC2, and PC3 for Fourier coefficients. (a) Plots of PC1, PC2; (b) Plots of PC1, PC3. Red represents *E. gutta* from Southwestern China, purple from the Germanic Basin (Kozur & Seidel, 1983a) and green from the Moscow Syncline together with the Germanic basin (Scholze et al., 2015; Scholze et al., 2016)

10–20 growth lines; ornamentation on growth bands is finely pitted to weakly reticulated; anterior and posterior margins sharply curved; position of the maximal curvature of anterior margin median-ventral to median-dorsal, at the posterior margin median-ventral, and at the ventral margin median-anterior to median-posterior. Among these features, the shape and linear measurements of *E. gutta* are variable, possibly caused by intraspecific variation, while the most important feature is the strongly convex larval valve and the significant finely pitted to weakly reticulated ornamentation on the growth bands.

Occurrence

Kayitou Formation in Western Guizhou and East Yunnan (Chu et al., 2013; Chu et al., 2016); middle part of the Sunjiagou Formation in North China (Chu et al., 2019); upper part of the Fulda Formation, lower part of the Calvörde Formation and Bernburg Formation in the Germanic Basin (Kozur & Weems, 2010; Scholze et al., 2015; Scholze et al., 2016); Vokhma Formation in the Moscow Syncline (Scholze et al., 2015).

4.2 | Other fossils

Abundant *Gigantopteris* flora plant fossils were recovered from various horizons below the last occurrence of the coal bed in the Xuanwei Formation of the studied sections, such as *Gigantopteris*, *Gigantonoclea*, *Lobatannularia*, *Annularia*, *Paracalamites*, *Fascipteris*, and *Pecopteris* (Figure 6). The *Gigantopteris* flora consists of more than 30 species in the upper part of the Xuanwei Formation in the Chahe section. Fourteen genera and 20 species of plant fossils belonging to the *Gigantopteris* flora were discovered at the base of the Kayitou Formation, which represents the last occurrence of the *Gigantopteris* flora at this site (Chu et al., 2016; Figure 7). In the Chinahe and Jinzhong sections, the *Gigantopteris* flora disappeared at the top of the Xuanwei Formation, associated with the absence of coal beds (Figure 7). Meanwhile, we collected *Annalepis*, *Peltaspermum*, and rare *Gigantopteris* flora remains in the Kayitou Formation of the three studied sections.

In the Jinzhong and Chinahe sections, the Kayitou Formation represents a shallow coastal lagoon evolving towards coastal transitional deposition and it has yielded a mixed continental-marine biota including bivalves, brachiopods (lingulids), spinicaudatans, and plants. The bivalves are *Pteria* cf. *ussurica*, *Neoschizodus orbicularis*, *Neoschizodus laevigatus*, *Promyalina schamarae*, *Promyalina putiatinensis*, and *Permophorus bregeri*, and they were collectively named the *Pteria-Neoschizodus-Promyalina* assemblage. Meanwhile, abundant lingulid brachiopods occur at different levels in the Kayitou Formation in the Jinzhong and Chinahe sections.

Additionally, we found abundant charcoal fossils in the Kayitou Formation, and observations under the SEM show that the charcoal preserves typical anatomical details and homogenized cell walls (Figure 6).

4.3 | Organic carbon isotopes

The organic carbon $\delta^{13}C$ curves of the three studied sections show similar marked shifts and trends (Figure 7). In the Chahe section, $\delta^{13}C_{org}$ values of bulk organic matter in the Xuanwei Formation and the lowest Kayitou Formation are stable, with a range from around −24‰ to −23‰. Subsequently, a dramatic decrease of about 5‰ in $\delta^{13}C_{org}$ of bulk organic matter occurred in the lower part of the Kayitou Formation, with a range from around −29‰ to −26‰ through the negative carbon isotope excursion (CIE) (Figure 7). A comparable pattern is observed in the Chinahe section. Bulk $\delta^{13}C_{org}$ values from the Xuanwei Formation are around −25‰ to −24‰.

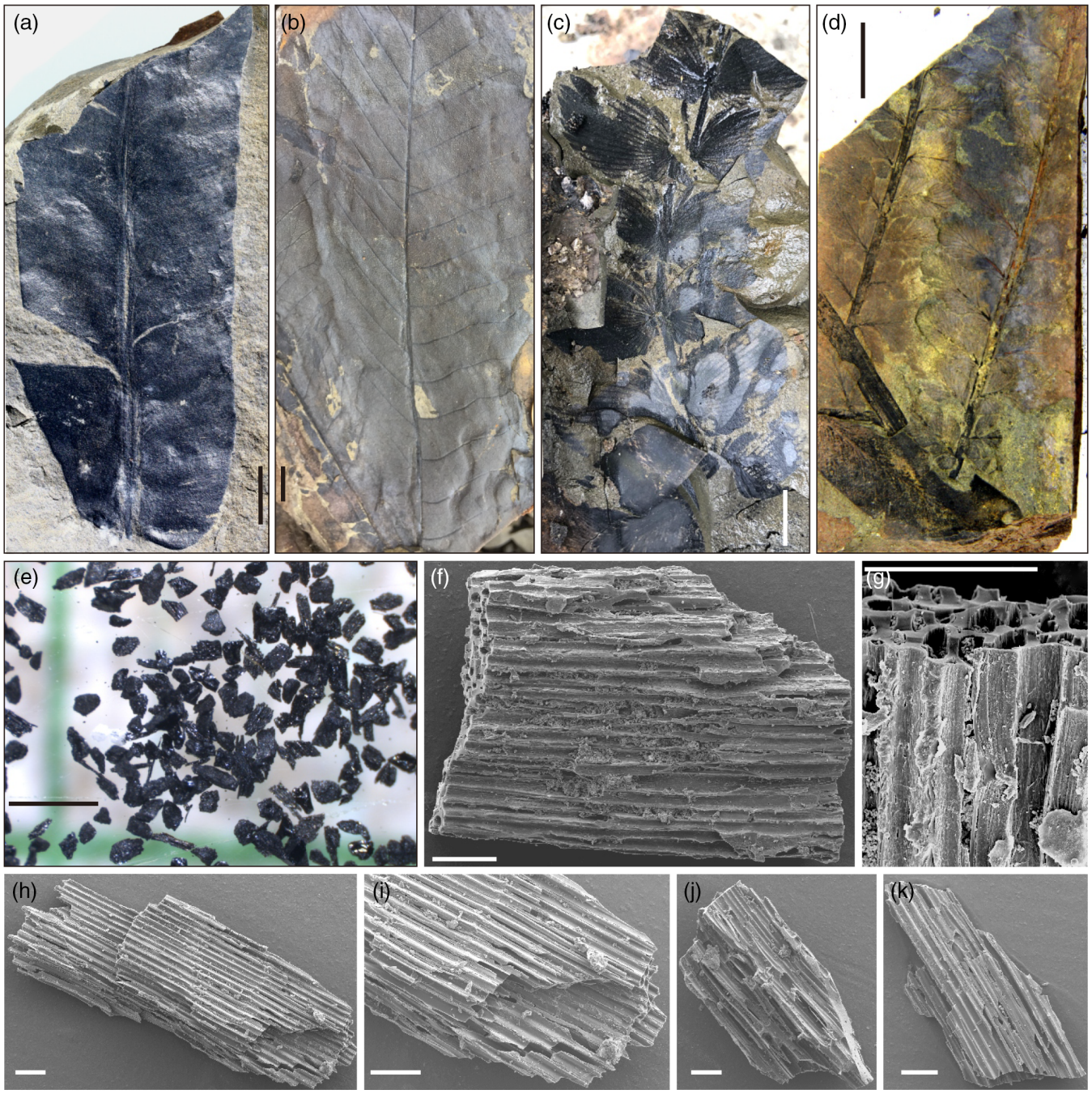

FIGURE 6 Typical *Gigantopteris* flora (Xuanwei Formation) and charcoal fossils (Kayitou Formation) from the Chinahe section. (a) *Compsopteris contracta*; (b) *Gigantopteris dictyophylloides*; (c) *Lobatannularia* sp.; (d) *Pecopteris* sp.; (e) charcoal particles under binocular microscope; (f–k) SEM images showing the typical anatomical details on the charcoal. (a), (b), (f), (g) are from supplementary of Chu et al. (2020). Scale bars are 1 cm (a–d), 1 mm (e–g), or 100 μm (h–k)

Then, $\delta^{13}C_{org}$ values decrease at the top of the Xuanwei Formation, followed by a stepwise negative CIE (∼ – 5‰) in the Kayitou Formation. In the Jinzhong section, bulk $\delta^{13}C_{org}$ values from the Xuanwei Formation are around −25‰ to −24‰. A negative shift of about −5‰ in $\delta^{13}C_{org}$ of bulk organic matter occurred at the base of the Kayitou Formation. The $\delta^{13}C_{org}$ values of the three studied sections show a slight positive shift in the uppermost Kayitou Formation and the lower part of the Dongchuan Formation. The onset of the CIE is the time from the last samples with pre-CIE carbon isotope composition to the first most depleted values, corresponding to the intervals from 87.5 to 89.0 m at Chahe, 25.0 to 28.5 m at Chinahe, and 28.0 to 35.0 m at Jinzhong.

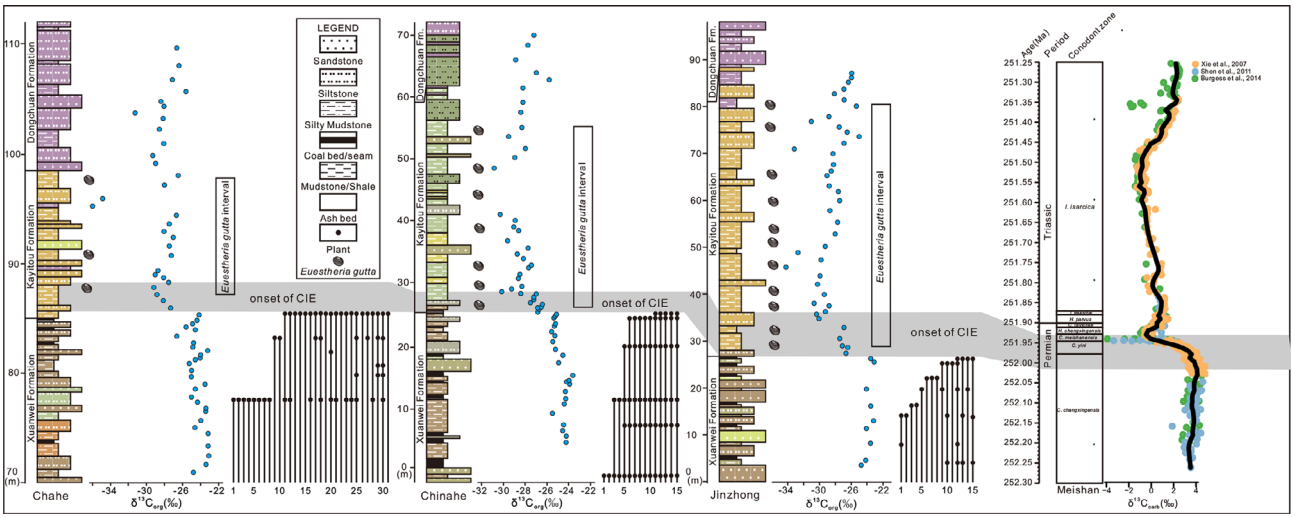

FIGURE 7 The distribution of *Gigantopteris* flora plant fossils, *E. gutta* and organic carbon isotopes data from the studied sections (Plant fossil data of Chahe and Jinzhong sections are from Chu et al., 2016; Plant fossil data of Chinahe section are modified from Chu et al., 2020; Organic carbon isotopes data of Chahe and Chinahe sections are from Shen, Crowley, et al., 2011 and Chu et al., 2020). The log shows lithologies with approximate representation of colour for rocks. The list of the fossils is provided in the electronic Supplementary material

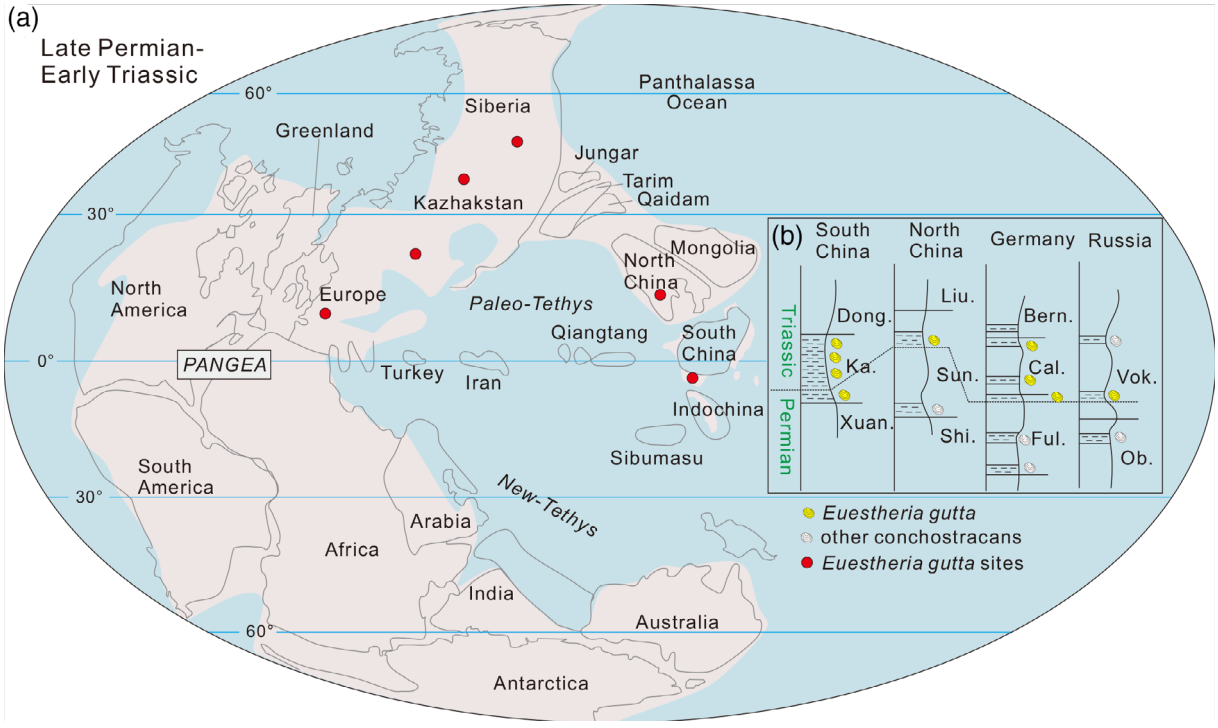

FIGURE 8 Palaeogeographical distribution of *E. gutta*. (a) Late Permian to Early Triassic palaeogeographical map showing that*E. gutta* has been widely reported from the northern hemisphere (base palaeogeographical map after Muttoni et al., 2009); (b) general lithological logs showing the horizons of the *E. gutta* appearances during the P–Tr transition in South China, North China, Germany and Russia (see the discussion in the main text). Xuan., Xuanwei Formation; Ka., Kayitou Formation; Dong., Dongchuan Formation; Shi., Shihezi Formation; Sun., Sunjiagou Formation; Liu., Liujiagou Formation; Ful., Fulda Formation; Cal., Calvörde Formation; Bern., Bernberg Formation; Ob, Obnora Formation; Vok., Vokhma Formation

5 | DISCUSSION

5.1 | *Euestheria gutta* occurred within the continental mass extinction interval in South China

The time range of *E. gutta* has attracted attention in continental P–Tr biostratigraphic studies, especially in the Germanic Basin. It was first discovered below the base of the Buntsandstein and thought to be latest Changhsingian in age, then dominated in the lowermost Buntsandstein near the P–Tr boundary, while it could be rare in Lower Triassic strata (e.g., Kozur & Weems, 2010). However, a reinvestigation of spinicaudatans from the Late Permian to Early Triassic in central Germany proposed that the age of *E. gutta* coupled with other species is Early Triassic and the position of the P–Tr boundary was lowered to the top of the Zechstein Group, based on comparison with the Early Triassic spinicaudatan record in the Moscow Syncline (Scholze et al., 2016). Furthermore, this conclusion was confirmed by further multistratigraphic study, including chemostratigraphy, magnetostratigraphy, and palynology (Scholze et al., 2017). However, the data from both the Germanic Basin and Moscow Syncline cannot be correlated with the marine record, which means that the time range of *E. gutta* still has to be resolved. Meanwhile, the temporal relation between the occurrence of *E. gutta* and the mass extinction is debatable, and it would make more sense to indicate the interval of continental biotic crisis.

In the present studied area, a dramatic reduction in the diversity of the *Gigantopteris* flora and the absence of coals were observed at the base of the Kayitou Formation or the uppermost part of the Xuanwei Formation (Chu et al., 2016; Shen, Crowley, et al., 2011; Zhang et al., 2016). Generally, major P–Tr floral and faunal turnovers are accompanied by a negative CIE observed globally in both carbonate and organic matter (e.g., Korte & Kozur, 2010), and always regarded as the mark of the Permian-Triassic mass extinction (PTME) (Tong et al., 2019). Our results show a negative excursion of ~5 to 6‰ and that the onset of the negative CIE occurred simultaneously with the loss of plants in the studied sections (Figure 7). The marked negative shifts in $\delta^{13}C_{org}$ that we observed should be consistent with both the global organic and inorganic carbon isotope records and represent global carbon cycle perturbations during the PTME (e.g., Fielding et al., 2019; Grasby et al., 2011; Shen, Sun, et al., 2011). And the negative CIE represents global carbon cycle perturbations and a significant injection of ^{13}C-depleted C during the PTME. Generally, it was associated with thermogenic CO_2 release from organic-rich sediments intruded by the Siberian Traps. In addition, abundant fossil charcoal is observed following the onset of the negative CIE, suggesting increased wildfire activity in this area during the P–Tr transition (Chu et al., 2020). This increase in wildfire activity probably affected all South China, as anomalously high concentrations of combustion-derived polynuclear aromatic hydrocarbons (PAHs) and black carbon (BC) are also found in the event beds of Meishan (Shen, Sun, et al., 2011; Xie et al., 2007).

Hence, these results indicate that the continental mass extinction was represented by the dramatic loss of the rainforest-type *Gigantopteris* flora coincident with the onset of a negative CIE in South China, and extensive wildfire activity might have contributed to the disturbance in peatlands and the collapse of tropical continental ecosystems. Subsequently, abundant *E. gutta* were collected in the Kayitou Formation, and its first occurrence was observed at the onset of the negative CIE and just above the horizon of the loss of the *Gigantopteris* flora, which means that it could be regarded as a marker of the P–Tr transitional interval (Figure 7).

5.2 | The palaeogeographical distribution and palaeoecology of *Euestheria gutta*

E. gutta was first described from the Rybinskian Horizon of the Vetlugian Series in both the Moscow Syncline (Lutkevich, 1937) and Siberia (Lutkevich, 1938), which is regarded as Early Triassic in age. *E. gutta* was reported from the Fulda, Calvörde, and Bernberg formations in central Germany (Kozur & Seidel, 1983a, 1983b; Kozur & Weems, 2010), and these have been verified by subsequent studies (Scholze et al., 2016; Scholze et al., 2017), though the age of its first appearance is controversial. Recently, *E. gutta* were reported from the Kayitou Formation in southwestern China (Chu et al., 2013; Chu et al., 2016; Scholze et al., 2019). Furthermore, Scholze et al. (2015) documented *E. gutta* in association with *Magniestheria mangaliensis* from the Vokhma Formation (Vokhmian Regional Stage; Early Triassic) in the Moscow Syncline, and a similar spinicaudatan assemblage also appeared in North China (Chu et al., 2019). In summary, *E. gutta* has been widely reported from various basins in the northern hemisphere (Figure 8), but spinicaudatans have not been widely studied, and there are no reported occurrences of *E. gutta* in the southern hemisphere. Even so, the wide distribution of this species in the northern hemisphere suggests that it has great potential for biostratigraphic correlation among various continental basins. According to current reports of the occurrences of *E. gutta*, its time range was from latest Permian to earliest Triassic, and the *E. gutta* spinicaudatan fauna or *E. gutta* interval corresponds to the P–Tr transitional interval.

Modern spinicaudatans occur in inland freshwater, saline ponds, and lakes, brackish estuaries (Martínez-Pantoja et al., 2002) and even coastal lagoons, and their minute eggs may be transported by the wind, currents, or insects (Schneider & Scholze, 2016). Their resting eggs can hatch and develop rapidly to the adult when environmental conditions improve, which results in widespread environmental distribution (Benvenuto, Calabrese, Reed, & Knott, 2009). Moreover, fossil clam shrimps can live in brackish environments and deltaic marginal marine or permanent and deep water bodies, such as very shallow marine deposits (Kozur & Weems, 2010; Scholze et al., 2016). The Permian–Triassic transitional clam shrimp most likely lived in places that were affected by local water flow and interregional wind transport (Scholze et al., 2016). In the present study, *E. gutta* was discovered associated with brackish bivalves and brachiopods in the same horizons of the Kayitou Formation from the Jinzhong and Chinahe sections (Chu et al., 2016). The well-preserved carapaces of bivalves and brachiopods (even right and left valves preserved together) in the

laminated mudstone suggested they were not transported over long distances. Hence, our results show that *E. gutta* could live in brackish coastal waters. Combined with previous studies, we propose that *E. gutta* was a euryhaline species, and it could be distributed in typical intracontinental basins and coastal lagoon facies. Additionally, the wide geographic distribution of *E. gutta* might result from the transportation of their eggs by the wind on land and currents along the coastline.

6 | CONCLUSIONS

The position of the continental PTB is disputed and it is difficult to explore biostratigraphic correlation among continental deposits because of the absence of eurytopic markers. Spinicaudatans are some of the most common fossils in continental strata and they have been considered as potential index fossils for continental stratigraphic division and correlation. In this study, we document the detailed morphology and biostratigraphic significance of *E. gutta* based on well-preserved fossils from southwestern China. The linear measurements and Fourier shape analysis of *E. gutta* show significant intraspecific variation, while the strongly convex larval valve and the finely pitted to weakly reticulated ornamentation on growth bands were the most important identifying characteristics. There is also strong intraspecific morphological variation among *E. gutta* specimens from different regions, and differences in the shape of the dorsal margin are the most significant variable trait. Evidence from palaeobotany, organic carbon isotopes, and charcoal indicates that the continental mass extinction in South China was marked by the loss of tropical rainforest vegetation and a negative CIE coupled with enhanced wildfire events during the P–Tr transition. Meanwhile, the *E. gutta* spinicaudatan fauna was observed at the onset of the negative CIE and just above the horizon of loss of the *Gigantopteris* flora. We conclude that *E. gutta* could be considered as a biostratigraphical index fossil of the continental mass extinction interval or P–Tr transitional beds, present in the latest Permian and the earliest Triassic.

ACKNOWLEDGEMENTS

We thank Xincheng Qiu, Wenwei Guo, and Ting Song who helped with hunting fossils from the studied sections. Hao Yang and Enhao Jia are thanked for assistance with obtaining SEM images. We thank Huanyu Liao for valuable comments on earlier version of this manuscript. The authors are grateful to Manja Hethke, the anonymous reviewer and editor Zhong-Qiang Chen for their constructive comments and suggestions. This study was supported by the National Natural Science Foundation of China (42072025, 41702015, 41802031) and the China Geological Survey (CDD2001-03, DD20190009). This article is dedicated to the memory of Professor Zhuoting Liao.

PEER REVIEW

The peer review history for this article is available at https://publons.com/publon/10.1002/gj.4096.

DATA AVAILABILITY STATEMENT

The data that supports the findings of this study are available in the supplementary material of this article.

REFERENCES

Astrop, T. I., Sahni, V., Blackledge, T. A., & Stark, A. Y. (2015). Mechanical properties of the chitin-calcium-phosphate "clam shrimp" carapace (Branchiopoda: Spinicaudata): Implications for taphonomy and fossilization. *Journal of Crustacean Biology*, *35*, 123–131. https://doi.org/10.1163/1937240X-00002332.

Benton, M. J. (2015). *When life nearly died: The greatest mass extinction of all time* (2nd ed., p. 352). London: Thames & Hudson.

Benton, M. J., Tverdokhlebov, V. P., & Surkov, M. V. (2004). Ecosystem remodelling among vertebrates at the Permian–Triassic boundary in Russia. *Nature*, *432*, 97–100. https://doi.org/10.1038/nature02950.

Benvenuto, C., Calabrese, A., Reed, S. K., & Knott, B. (2009). Multiple hatching events in clam shrimp: Implications for mate guarding behaviour and community ecology. *Current Science*, *96*, 130–136 https://www.jstor.org/stable/24104740.

Bercovici, A., Cui, Y., Forel, M. B., Yu, J., & Vajda, V. (2015). Terrestrial paleoenvironment characterization across the Permian–Triassic boundary in South China. *Journal of Asian Earth Sciences*, *98*, 225–246. https://doi.org/10.1016/j.jseaes.2014.11.016.

Botha, J., & Smith, R. M. (2006). Rapid vertebrate recuperation in the Karoo Basin of South Africa following the end-Permian extinction. *Journal of African Earth Sciences*, *45*, 502–514.

Burgess, S. D., Bowring, S., & Shen, S. (2014). High-precision timeline for Earth's most severe extinction. *Proceedings of the National Academy of Sciences*, *111*, 3316–3321. https://doi.org/10.1073/pnas.1317692111.

Burgess, S. D., Muirhead, J. D., & Bowring, S. A. (2017). Initial pulse of Siberian Traps sills as the trigger of the end-Permian mass extinction. *Nature Communications*, *8*, 164.

Cao, C., Wang, W., Liu, L., Shen, S., & Summons, R. E. (2008). Two episodes of ^{13}C-depletion in organic carbon in the latest Permian: evidence from the terrestrial sequences in northern Xinjiang, China. *Earth and Planetary Science Letters*, *270*, 251–257.

Chen, J., & Xu, Y. (2019). Establishing the link between Permian volcanism and biodiversity changes: Insights from geochemical proxies. *Gondwana Research*, *75*, 68–96. https://doi.org/10.1016/j.gr.2019.04.008.

Chen, Z. Q., Yang, H., Luo, M., Benton, M. J., Kaiho, K., Zhao, L., … Chen, L. (2015). Complete biotic and sedimentary records of the Permian–Triassic transition from Meishan section, South China: Ecologically assessing mass extinction and its aftermath. *Earth-Science Reviews*, *149*, 67–107.

Chu, D., Grasby, S. E., Song, H., Dal Corso, J., Wang, Y., Mather, T. A., … Wignall, P. B. (2020). Ecological disturbance in tropical peatlands prior to marine Permian-Triassic mass extinction. *Geology*, *48*, 288–292. https://doi.org/10.1130/G46631.1.

Chu, D., Tong, J., Benton, M. J., Yu, J., & Huang, Y. (2019). Mixed continental-marine biotas following the Permian-Triassic mass extinction in South and North China. *Palaeogeography, Palaeoclimatology, Palaeoecology*, *519*, 95–107. https://doi.org/10.1016/j.palaeo.2017.10.028.

Chu, D., Yu, J., Tong, J., Benton, M. J., Song, H., Huang, Y., … Tian, L. (2016). Biostratigraphic correlation and mass extinction during the Permian-Triassic transition in terrestrial-marine siliciclastic settings of South China. *Global and Planetary Change*, *146*, 67–88. https://doi.org/10.1016/j.gloplacha.2016.09.009.

Chu, D. L., Tong, J. N., Yu, J. X., Song, H. J., & Tian, L. (2013). The conchostracan fauna from the Kayitou Formation of Western Guizhou, China. *Acta Palaeontologica Sinica*, *52*, 265–280 (In Chinese with English abstract).

Defretin-Lefranc, S. (1965). Etude et révision de Phyllopodes Conchostracés en provenance d'U.R.S.S. *Annales de la Société Géologique du Nord*, *85*, 15–48.

Erwin, D. H. (2006). *How life on earth nearly ended 250 million years ago* (p. 320). Princeton: Princeton University Press.

Fielding, C. R., Frank, T. D., McLoughlin, S., Vajda, V., Mays, C., Tevyaw, A. P., … Crowley, J. L. (2019). Age and pattern of the southern high-latitude continental end-Permian extinction constrained by multiproxy analysis. *Nature Communications*, *10*, 385. https://doi.org/10.1038/s41467-018-07934-z.

Gastaldo, R. A., Kamo, S. L., Neveling, J., Geissman, J. W., Bamford, M., & Looy, C. V. (2015). Is the vertebrate-defined Permian-Triassic boundary in the Karoo Basin, South Africa, the terrestrial expression of the end-Permian marine event? *Geology*, *43*, 939–942. https://doi.org/10.1130/G37040.1.

Gastaldo, R. A., Kamo, S. L., Neveling, J., Geissman, J. W., Looy, C. V., & Martini, A. M. (2020). The base of the *Lystrosaurus* Assemblage Zone, Karoo Basin, predates the end-Permian marine extinction. *Nature Communications*, *11*, 1428.

Gastaldo, R. A., Knight, C. L., Neveling, J., & Tabor, N. J. (2014). Latest Permian paleosols from Wapadsberg Pass, South Africa: Implications for Changhsingian climate. *Bulletin*, *126*, 665–679. https://doi.org/10.1130/B30887.1.

Grasby, S. E., Sanei, H., & Beauchamp, B. (2011). Catastrophic dispersion of coal fly ash into oceans during the latest Permian extinction. *Nature Geoscience*, *4*, 104–107. https://doi.org/10.1038/ngeo1069.

Haines, A. J., & Crampton, J. S. (2000). Improvements to the method of Fourier shape analysis as applied in morphometric studies. *Palaeontology*, *43*, 765–783. https://doi.org/10.1111/1475-4983.00148.

Hethke, M., Fürsich, F. T., Jiang, B., Wang, B., Chellouche, P., & Weeks, S. C. (2019). Ecological stasis in Spinicaudata (Crustacea, Branchiopoda)? Early Cretaceous clam shrimp of the Yixian Formation of north-east China occupied a broader realized ecological niche than extant members of the group. *Palaeontology*, *62*, 483–513.

Hethke, M., Fürsich, F. T., Morton, J. D., & Jiang, B. (2018). Analysis of morphological variability in the clam shrimp Eoestheria middendorfii (Crustacea, Spinicaudata) from the Lower Cretaceous of China, and its implications for spinicaudatan taxonomy. *Papers in Palaeontology*, *4*, 21–53.

Hethke, M., & Weeks, S. C. (2020). Population density effects on carapace growth in clam shrimp: Implications for palaeontological studies. *Zoological Studies*, *59*, e33.

Huang, D. (2019). Jurassic integrative stratigraphy and timescale of China. *Science China Earth Sciences*, *62*, 223–255. https://doi.org/10.1007/s11430-017-9268-7.

Joachimski, M. M., Lai, X., Shen, S., Jiang, H., Luo, G., Chen, B., … Sun, Y. (2012). Climate warming in the latest Permian and the Permian–Triassic mass extinction. *Geology*, *40*, 195–198. https://doi.org/10.1130/G32707.1.

Jones, R. (1862). *A monograph of the fossil Estheriae* (p. 150). London: Palaeontographical Society.

Korte, C., & Kozur, H. W. (2010). Carbon-isotope stratigraphy across the Permian–Triassic boundary: A review. *Journal of Asian Earth Sciences*, *39*, 215–235. https://doi.org/10.1016/j.jseaes.2010.01.005.

Kozur, H., & Seidel, G. (1983a). Revision der Conchostracen-Faunen des unteren und mittleren Buntsandsteins. *Teil I. Zeitschrift für Geologische Wissenschaften*, *11*, 289–417.

Kozur, H., & Seidel, G. (1983b). Die Biostratigraphie des unteren und mittleren Buntsandsteins des Germanischen Beckens unter besonderer Berücksichtigung der Conchostracen. Teil II zur Revision der Conchostracen-Faunen des unteren und mittleren Buntsandsteins. *Zeitschrift für Geologische Wissenschaften*, *11*, 429–464.

Kozur, H. W., & Weems, R. E. (2010). The biostratigraphic importance of conchostracans in the continental Triassic of the northern hemisphere. *Geological Society, London, Special Publications*, *334*, 315–417. https://doi.org/10.1144/SP334.13.

Kozur, H. W., & Weems, R. E. (2011). Detailed correlation and age of continental late Changhsingian and earliest Triassic beds: implications for the role of the Siberian Trap in the Permian–Triassic biotic crisis. *Palaeogeography, Palaeoclimatology, Palaeoecology*, *308*, 22–40. https://doi.org/10.1016/j.palaeo.2011.02.020.

Lucas, S. G. (2006). Global Permian tetrapod biostratigraphy and biochronology. *Geological Society, London, Special Publications*, *265*, 65–93. https://doi.org/10.1144/GSL.SP.2006.265.01.04.

Lucas, S. G. (2010). The Triassic timescale based on nonmarine tetrapod biostratigraphy and biochronology. *Geological Society, London, Special Publications*, *334*, 447–500. https://doi.org/10.1144/SP334.15.

Lutkevich, E. M. (1937). O nekotorych Phyllopoda SSSR (On some Phyllopoda of the USSR). *Ezhegodnik Vsesoyuznogo Paleontologicheskogo Obshchestva*, *11*, 60–70 (in Russian).

Lutkevich, E. M. (1938). Triassic Estheriae from the Upper Strata of the Tungussk series. *Transactions of the Arctic Institute*, *101*, 155–164.

Martínez-Pantoja, M. A., Alcocer, J., & Maeda-Martínez, A. M. (2002). On the Spinicaudata (Branchiopoda) from Lake Cuitzeo, Michoacán, México: First report of a clam shrimp fishery. *Hydrobiologia*, *486*, 207–213.

Metcalfe, I., Crowley, J. L., Nicoll, R. S., & Schmitz, M. (2015). High-precision U-Pb CA-TIMS calibration of Middle Permian to Lower Triassic sequences, mass extinction and extreme climate-change in eastern Australian Gondwana. *Gondwana Research*, *28*, 61–81. https://doi.org/10.1016/j.gr.2014.09.002.

Morton, J. D., Whiteside, D. I., Hethke, M., & Benton, M. J. (2017). Biostratigraphy and geometric morphometrics of conchostracans (Crustacea, Branchiopoda) from the Late Triassic fissure deposits of Cromhall Quarry, UK. *Palaeontology*, *60*, 349–374. https://doi.org/10.1111/pala.12321.

Muttoni, G., Gaetani, M., Kent, D. V., Sciunnach, D., Angiolini, L., Berra, F., … Zanchi, A. (2009). Opening of the Neo-Tethys Ocean and the Pangea B to Pangea A transformation during the Permian. *GeoArabia*, *14* (4), 17–48.

Neveling, J., Gastaldo, R. A., Kamo, S. L., Geissman, J. W., Looy, C. V., & Bamford, M. K. (2016). A review of stratigraphic, geochemical, and paleontologic data of the terrestrial end-Permian record in the Karoo Basin, South Africa. In *Origin and evolution of the Cape Mountains and Karoo Basin* (pp. 151–157). Cham: Springer.

Nowak, H., Schneebeli-Hermann, E., & Kustatscher, E. (2019). No mass extinction for land plants at the Permian–Triassic transition. *Nature Communications*, *10*, art. 384. https://doi.org/10.1038/s41467-018-07945-w

Peng, Y., & Shi, G. R. (2009). Life crises on land across the Permian–Triassic boundary in South China. *Global and Planetary Change*, *65*, 155–165. https://doi.org/10.1016/j.gloplacha.2008.10.016.

Peng, Y., Zhang, S., Yu, T., Yang, F., Gao, Y., & Shi, G. R. (2005). High-resolution terrestrial Permian–Triassic eventostratigraphic boundary in western Guizhou and eastern Yunnan, southwestern China. *Palaeogeography, Palaeoclimatology, Palaeoecology*, *215*, 285–295. https://doi.org/10.1016/j.palaeo.2004.09.009.

Rohlf, F. (2010). *TpsDig, digitize landmarks and outlines, v.2.16*, Department of Ecology & Evolution, State University of New York at Stony Brook.

Schneider, J. W., Lucas, S. G., Scholze, F., Voigt, S., Marchetti, L., Klein, H., … Shen, S. (2020). Late Paleozoic–Early Mesozoic continental biostratigraphy—Links to the Standard Global Chronostratigraphic Scale. *Palaeoworld*, *29*, 186–238. https://doi.org/10.1016/j.palwor.2019.09.001.

Schneider, J. W., & Scholze, F. (2016). Late Pennsylvanian–Early Triassic conchostracan biostratigraphy: A preliminary approach. *Geological Society, London, Special Publications*, *450*, 365–386. https://doi.org/10.1144/SP450.6.

Scholze, F., Golubev, V. K., Niedźwiedzki, G., Schneider, J. W., & Sennikov, A. G. (2019). Late Permian conchostracans (Crustacea,

Branchiopoda) from continental deposits in the Moscow syneclise, Russia. *Journal of Paleontology*, *93*, 72–97. https://doi.org/10.1017/jpa.2018.58.

Scholze, F., Golubev, V. K., Niedźwiedzki, G., Sennikov, A. G., Schneider, J. W., & Silantiev, V. V. (2015). Early Triassic conchostracans (Crustacea: Branchiopoda) from the terrestrial Permian–Triassic boundary sections in the Moscow syncline. *Palaeogeography, Palaeoclimatology, Palaeoecology*, *429*, 22–40. https://doi.org/10.1016/j.palaeo.2015.04.002.

Scholze, F., Schneider, J. W., & Werneburg, R. (2016). Conchostracans in continental deposits of the Zechstein–Buntsandstein transition in central Germany: Taxonomy and biostratigraphic implications for the position of the Permian–Triassic boundary within the Zechstein Group. *Palaeogeography, Palaeoclimatology, Palaeoecology*, *449*, 174–193. https://doi.org/10.1016/j.palaeo.2016.02.021.

Scholze, F., Wang, X., Kirscher, U., Kraft, J., Schneider, J. W., Götz, A. E., … Bachtadse, V. (2017). A multistratigraphic approach to pinpoint the Permian-Triassic boundary in continental deposits: The Zechstein–Lower Buntsandstein transition in Germany. *Global and Planetary Change*, *152*, 129–151. https://doi.org/10.1016/j.gloplacha.2017.03.004.

Shen, S. Z., Crowley, J. L., Wang, Y., Bowring, S. A., Erwin, D. H., Sadler, P. M., … Jin, Y. (2011). Calibrating the end-Permian mass extinction. *Science*, *334*, 1367–1372. https://doi.org/10.1126/science.1213454.

Shen, W., Sun, Y., Lin, Y., Liu, D., & Chai, P. (2011). Evidence for wildfire in the Meishan section and implications for Permian–Triassic events. *Geochimica et Cosmochimica Acta*, *75*, 1992–2006. https://doi.org/10.1016/j.gca.2011.01.027.

Smith, R. M., & Ward, P. D. (2001). Pattern of vertebrate extinctions across an event bed at the Permian-Triassic boundary in the Karoo Basin of South Africa. *Geology*, *29*, 1147–1150. https://doi.org/10.1130/0091-7613(2001)029<1147:poveaa>2.0.co;2.

Song, H., Wignall, P. B., Tong, J., & Yin, H. (2013). Two pulses of extinction during the Permian–Triassic crisis. *Nature Geoscience*, *6*, 52–56. https://doi.org/10.1038/ngeo1649.

Song, T., Tong, J., Tian, L., Chu, D., & Huang, Y. (2019). Taxonomic and ecological variations of Permian-Triassic transitional bivalve communities from the littoral clastic facies in southwestern China. *Palaeogeography, Palaeoclimatology, Palaeoecology*, *519*, 108–123. https://doi.org/10.1016/j.palaeo.2018.02.027.

Steiner, M. B. (2006). The magnetic polarity time scale across the Permian-Triassic boundary. *Geological Society, London, Special Publications*, *265*, 15–38. https://doi.org/10.1144/GSL.SP.2006.265.01.02.

Szurlies, M. (2007). Latest Permian to Middle Triassic cyclomagnetostratigraphy from the Central European Basin, Germany: implications for the geomagnetic polarity timescale. *Earth and Planetary Science Letters*, *261*, 602–619. https://doi.org/10.1016/j.epsl.2007.07.018.

Szurlies, M. (2013). Late Permian (Zechstein) magnetostratigraphy in western and central Europe. *Geological Society, London, Special Publications*, *376*, 73–85. https://doi.org/10.1144/SP376.7.

Tasch, P. (1987). Fossil Conchostraca of the southern hemisphere and continental drift, paleontology, biostratigraphy, and dispersal. *The Geological Society of America Memoir*, *165*, 1–290.

Tasch, P., & Volkheimer, W. (1970). Jurassic conchostracans from Patagonia. *The University of Kansas Paleontology Contributions*, *50*, 1–23.

Taylor, G. K., Tucker, C., Twitchett, R. J., Kearsey, T., Benton, M. J., Newell, A. J., … Tverdokhlebov, V. P. (2009). Magnetostratigraphy of Permian/Triassic boundary sequences in the Cis-Urals, Russia: No evidence for a major temporal hiatus. *Earth and Planetary Science Letters*, *281*, 36–47. https://doi.org/10.1016/j.epsl.2009.02.002.

Tong, J., Chu, D., Liang, L., Shu, W., Song, H., Song, T., … Wu, Y. (2019). Triassic integrative stratigraphy and timescale of China. *Science China Earth Sciences*, *62*, 189–222. https://doi.org/10.1007/s11430-018-9278-0.

Twitchett, R. J., Looy, C. V., Morante, R., Visscher, H., & Wignall, P. B. (2001). Rapid and synchronous collapse of marine and terrestrial ecosystems during the end-Permian biotic crisis. *Geology*, *29*, 351–354. https://doi.org/10.1130/0091-7613(2001)029<0351:rascom>2.0.co;2.

Viglietti, P. A., Smith, R. M., Angielczyk, K. D., Kammerer, C. F., Fröbisch, J., & Rubidge, B. S. (2016). The *Daptocephalus* Assemblage Zone (Lopingian), South Africa: A proposed biostratigraphy based on a new compilation of stratigraphic ranges. *Journal of African Earth Sciences*, *113*, 153–164. https://doi.org/10.1016/j.jafrearsci.2015.10.011.

Ward, P. D., Botha, J., Buick, R., De Kock, M. O., Erwin, D. H., Garrison, G. H., … Smith, R. (2005). Abrupt and gradual extinction among Late Permian land vertebrates in the Karoo Basin, South Africa. *Science*, *307*, 709–714. https://doi.org/10.1126/science.1107068.

Wignall, P. B. (2001). Large igneous provinces and mass extinctions. *Earth-Science Reviews*, *53*, 1–33. https://doi.org/10.1016/S0012-8252(00)00037-4.

Wignall, P. B., Chu, D., Hilton, J. M., Dal Corso, J., Wu, Y., Wang, Y., … Tong, J. (2020). Death in the shallows: The record of Permo-Triassic mass extinction in paralic settings, southwest China. *Global and Planetary Change*, *189*, 103176. https://doi.org/10.1016/j.gloplacha.2020.103176.

Wignall, P. B., & Hallam, A. (1992). Anoxia as a cause of the Permian/Triassic mass extinction: facies evidence from northern Italy and the western United States. *Palaeogeography, Palaeoclimatology, Palaeoecology*, *93*, 21–46. https://doi.org/10.1016/0031-0182(92)90182-5.

Wu, Y., Tong, J., Algeo, T. J., Chu, D., Cui, Y., Song, H., … Du, Y. (2020). Organic carbon isotopes in terrestrial Permian-Triassic boundary sections of North China: Implications for global carbon cycle perturbations. *Bulletin*, *132*, 1106–1118. https://doi.org/10.1130/B35228.1.

Xie, S., Pancost, R. D., Huang, X., Jiao, D., Lu, L., Huang, J., … Evershed, R. P. (2007). Molecular and isotopic evidence for episodic environmental change across the Permo/Triassic boundary at Meishan in South China. *Global and Planetary Change*, *55*, 56–65. https://doi.org/10.1016/j.gloplacha.2006.06.016.

Zhang, H., Cao, C., Liu, X., Mu, L., Zheng, Q., Liu, F., … Shen, S. (2016). The terrestrial end-Permian mass extinction in South China. *Palaeogeography, Palaeoclimatology, Palaeoecology*, *448*, 108–124. https://doi.org/10.1016/j.palaeo.2015.07.002.

SUPPORTING INFORMATION

Additional supporting information may be found online in the Supporting Information section at the end of this article.

How to cite this article: Miao X, Chu D, Tong J, et al. Biostratigraphic significance and geometric morphometrics of *Euestheria gutta* (Crustacea: Branchiopoda: Spinicaudata): An index fossil of continental Permian–Triassic transitional beds. *Geological Journal*. 2021;56:6176–6188. https://doi.org/10.1002/gj.4096